*San Sebastian — Guipuzcoa*

# PART I

# WAVES

*Playa y costa en Punta Fagelda — Pontevedera*

CHAPTER 1


NONLINEAR DIFFRACTION BY A VERTICAL CYLINDER

David L. Kriebel *


## ABSTRACT

A theoretical solution is developed for the interaction of second-order Stokes waves with a large vertical circular cylinder in water of finite depth. The solution is obtained in terms of the velocity potential such that any kinematic or dynamic quantity of interest may be derived, consistent to the second perturbation order. In this study, the second-order wave field around the cylinder is determined, showing the modification of the incident Stokes waves by wave-wave and wave-structure interactions, both in the reflection-dominated up-wave region and in the diffraction-dominated down-wave region. The theory is then compared to experimental data for wave runup and rundown amplitudes on the cylinder as well as for wave crest and trough envelopes in the up-wave and down-wave regions.


## INTRODUCTION

Over the past 15 years, numerous theories have been proposed for the problem of the interaction of second-order Stokes waves with a fixed vertical circular cylinder. The first-order problem - the linear diffraction theory - was solved by MacCamy and Fuchs (1954); however, the second-order problem has proven more difficult to solve and, at present, none of the proposed solution is universally accepted. A review of all previous theories for the nonlinear diffraction problem is beyond the scope of this paper. Some of the most recent second-order diffraction theories for a vertical cylinder include those of Chen and Hudspeth (1982), Hunt and Williams (1982), Rahman and Heaps (1983), and Sabuncu and Gören (1985), while Garrison (1978) presents a nonlinear diffraction theory for arbitrary fixed or floating bodies.

The goals of this paper are to review a theory for the second-order diffraction problem developed recently by the author and to present examples of the resulting second-order free surface and nonlinear wave runup. These features of the nonlinear free surface are found to differ significantly from the linear solution, unlike the second-order wave forces which most theories predict are only slightly larger than the forces derived from linear diffraction theory. Interestingly, few of the previous theories have considered second-order free surface features, despite the fact that the second-order free surface contains fundamental nonlinear effects for a very simple geometry that has been widely used in offshore construction.

* Ocean Engineering Program, United States Naval Academy, Annapolis, MD 21402

THEORETICAL DEVELOPMENT

    The problem under consideration consists of a fixed, vertical cylinder of radius, $a$, in water of uniform depth, $d$, subjected to nonlinear periodic waves of height, $H$, propagating in the positive $x$ direction as shown in Figure 1. It is assumed that the fluid is irrotational and incompressible such that a potential-flow solution may be obtained in terms of the velocity potential, $\Phi(r,\theta,z,t)$. This potential must then satisfy the Laplace equation plus appropriate kinematic and dynamic boundary conditions at the bottom, at the free surface, at the cylinder, and in the far field.
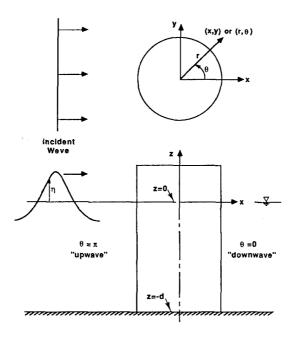


Figure 1. Definition sketch.

    Due to the complexity of the nonlinear boundary value problem, an approximate solution is sought through a perturbation expansion in which the velocity potential and the free surface elevation are expressed in series form as

$$\Phi = \Phi_1 + \Phi_2 + \cdots$$

$$\eta = \eta_1 + \eta_2 + \cdots \tag{1}$$

where the first-order term has a linear dependence on the wave steepness, $kH$, while the second-order term has a dependence like $(kH)^2$, where $k$ is the linear wavenumber. In addition, the free surface boundary conditions are expanded in a Taylor series about the still water level, $z = 0$. As a result, separate boundary value problems are obtained for each term in the perturbation expansion, $\Phi_1$ and $\Phi_2$.

At first-order, the solution must be obtained for the linear boundary value problem, which may be expressed as

$$\nabla^2 \Phi_1 = 0 \tag{2a}$$

$$\Phi_{1z} = 0 \quad \text{on } z = -d \tag{2b}$$

$$\Phi_{1tt} + g\Phi_{1z} = 0 \quad \text{on } z = 0 \tag{2c}$$

$$\Phi_{1r} = 0 \quad \text{on } r = a \tag{2d}$$

$$\lim_{r \to \infty} r^{1/2} \left( \Phi_{1r}^s - ik\Phi_1^s \right) = 0 \tag{2e}$$

where the combined free surface boundary condition, (2c), is particularly important since it governs the wavenumbers of the linear solution and since it changes dramatically at second-order. The general solution for this linear diffraction problem has been given by MacCamy and Fuchs (1954) as the real part of

$$\Phi_1 = -\frac{igH}{2\sigma} \frac{\cosh k(d+z)}{\cosh kd} \sum_{n=0}^{\infty} \beta_n \left[ J_n(kr) - \frac{J_n'(ka)}{H_n'(ka)} H_n(kr) \right] \cos n\theta \, e^{-i\sigma t} \tag{3}$$

where $\beta_n = (2 - \delta_{n0}) i^n$ and where $\delta_{n0}$ is the Kronecker delta function. In (3), the infinite series of Bessel functions $J_n(kr)$ represents linear incident plane waves while the Hankel functions $H_n(kr)$ represent outwardly-propagating linear scattered waves.

At second-order, the governing boundary value problem is considerably more complicated due to nonlinear forcing terms which appear in the free surface boundary condition. The second-order boundary value problem may be given by

$$\nabla^2 \Phi_2 = 0 \tag{4a}$$

$$\Phi_{2z} = 0 \quad \text{on } z = -d \tag{4b}$$

$$\Phi_{2tt} + g\Phi_{2z} = \frac{1}{g}\Phi_{1t} \left[ \Phi_{1ttz} + g\Phi_{1zz} \right]$$
$$- 2 \left[ \Phi_{1r}\Phi_{1rt} + \frac{1}{r^2}\Phi_{1\theta}\Phi_{1\theta t} + \Phi_{1z}\Phi_{1zt} \right] \quad \text{on } z = 0 \tag{4c}$$

$$\Phi_{2r} = 0 \quad \text{on } r = a \tag{4d}$$

and a form of the radiation condition, which is not well-posed for the second order problem. Because of the quadratic forcing terms on the right side of (4c), the second-order boundary value problem is nonhomogeneous. The second-order solution is therefore expected to have both particular solutions, which represent forced wave motions due to nonlinearity in the free surface boundary condition, as well as complementary or homogeneous solutions, which represent free scattered wave motions at second-order.

By substituting the first-order solution in (3) into the second-order free surface boundary condition in (4c), it is found that the quadratic forcing is periodic and oscillates at twice the frequency of the linear waves. The quadratic forcing is also an even function of $\theta$, such that (4c) may be rewritten in series form as

$$\Phi_{2tt} + g\Phi_{2z} = -i\frac{(gkH)^2}{8\sigma} \sum_{n=0}^{\infty} \left[ f_n^{II}(r) + f_n^{IS}(r) + f_n^{SS}(r) \right] \cos n\theta \, e^{-i2\sigma t} \tag{5}$$

Expressions for the radial functions $f_n^{II}(r)$, $f_n^{IS}(r)$, and $f_n^{SS}(r)$ are given by Hunt and Williams (1982), Sabuncu and Gören (1985), or Kriebel (1987), where each term represents a distinct nonlinear product term from the first order incident and scattered waves.

In (5), the $f_n^{II}$ term represents plane-wave forcing which leads to the expected second-order plane-wave component at wavenumber $2k$, as found in the usual Stokes second-order wave theory. This term would exist at second-order even if no cylinder were present and is the result of nonlinear self-interactions of the first-order incident waves. The remaining forcing terms, $f_n^{IS}$ and $f_n^{SS}$, are the result of nonlinear cross-interactions of the first-order incident and scattered waves and nonlinear self-interactions of the first-order scattered waves, respectively. These forcing terms behave much like a non-uniform pressure field applied to the free surface and they generate additional cylindrical standing and outwardly progressive waves at second-order.

The solution for the second-order velocity potential may be obtained by separating the potential $\Phi_2$ into particular solutions, $\Phi_2^P$, and complementary or homogeneous solutions, $\Phi_2^H$, as

$$\Phi_2 = \Phi_2^P + \Phi_2^H \tag{6}$$

Based on (5), the particular solution may be further separated as

$$\Phi_2^P = \Phi_{2P}^{II} + \Phi_{2P}^{IS} + \Phi_{2P}^{SS} \tag{7}$$

The component, $\Phi_{2P}^{II}$, then represents the forced wave motion generated by the $f_n^{II}$ forcing, which is the usual Stokes plane wave component given by the real part of

$$\Phi_{2P}^{II} = -i\frac{3g(kH)^2}{8\sigma}\frac{(\tanh^2 kd - 1)}{(2k\tanh 2kd - k_2\tanh k_2 d)}\frac{\cosh 2k(d+z)}{\cosh 2kd}\sum_{n=0}^{\infty}\beta_n J_n(2kr)\cos n\theta\, e^{-i2\sigma t} \tag{8}$$

The wavenumber $k_2$ is the characteristic free wavenumber for the second-order problem and satisfies the second-order dispersion relationship

$$4\sigma^2 = gk_2\tanh k_2 d \tag{9}$$

which can be obtained from the homogeneous form of the free surface boundary condition in (4c) or (5). It is found that $k_2$ approaches $4k$ in deep water but approaches $2k$ in shallow water, where $\Phi_{2P}^{II}$ becomes infinite due to resonant forcing in the free surface boundary condition, as is well known.

In the same way, other forced wave components exist in the "incident" wave field due to the remaining $f_n^{IS}$ and $f_n^{SS}$ forcing terms. The solution for these second-order forced waves is found in closed integral form based on a source distribution method, which may be formalized by application of either Green's theorem or through use of Hankel transforms. In this analysis, the solution is first obtained for an isolated point source of pressure oscillating on the free surface. This result is then generalized by integrating over the free surface in $r$ and $\theta$, to account for the distribution of the actual quadratic forcing found in the second-order free surface boundary condition. The solution follows that of Wehausen and Laitone (1960) for an arbitrary pressure distribution on the free surface; and, the resulting velocity potential due to the distributed forcing terms, $f_n^{IS}$ and $f_n^{SS}$, may be shown to be given by

$$\Phi_{2P}^{IS} + \Phi_{2P}^{SS} = -i\frac{g(kH)^2}{8\sigma k}\sum_{n=0}^{\infty}\cos n\theta\left[i2\pi\frac{k_2}{k}\frac{\cosh k_2 d\cosh k_2(d+z)}{\sinh 2k_2 d + 2k_2 d}J_n(k_2 r)D_n(k_2)\right.$$
$$\left. + PV\int_0^{\infty}\frac{\kappa\cosh\kappa(d+z)}{k\cosh\kappa d(\kappa\tanh\kappa d - k_2\tanh k_2 d)}J_n(\kappa r)D_n(\kappa)d\kappa\right]e^{-i2\sigma t} \tag{10}$$

where "PV" represents a Principal Value integral and where $D_n(\kappa)$ represents a wavenumber spectrum for cylindrical wave motions based on a Hankel transform as

$$D_n(\kappa) = \int_a^\infty r'\left[f_n^{IS}(r') + f_n^{SS}(r')\right] J_n(\kappa r') dr' \tag{11}$$

In the solution given by (10), the principal value integral represents standing wave motions based on a continuum of wavenumbers that are required to fit the complicated free surface boundary condition arising from the quadratic forcing. Away from the cylinder, however, only the second-order free wavenumber, $k_2$, is important and the integral term yields a cylindrical standing wave in the far field. From the source distribution method, the wave motions generated by any point source must satisfy the Sommerfeld radiation condition and yield outwardly propagating wave motions far from each source. Therefore, the additional term in the solution (10), represented by the component containing $J_n(k_2 r)$, is required so that the entire solution satisfies a form of the radiation condition.

The complicated forced-radiated waves given in (10), together with the incident bound second-harmonic given in (8), satisfy the nonlinear free surface boundary condition but do not satisfy the no-flow condition on the cylinder boundary by themselves. By allowing these waves to interact with the cylinder, second-order scattered waves must exist which are given by the complementary or homogeneous solutions in (6). These solutions must satisfy the Laplace equation, the bottom boundary condition, the Sommerfeld radiation condition, and the homogeneous form of the free surface boundary condition; and, they may be found from the general set of eigenfunction solutions for cylindrical waves as given by Dean and Dalrymple (1984) as

$$\Phi_2^H = \sum_{n=0} a_{n0} \cosh k_2(d + z) H_n(k_2 r) \cos n\theta$$
$$+ \sum_{n=0}\sum_{j=1} a_{nj} \cos \kappa_{2j}(d + z) K_n(\kappa_{2j} r) \cos n\theta\, e^{-i2\sigma t} \tag{12}$$

From the homogeneous form of the second-order free surface boundary condition, two second-order dispersion relationships result which specify the wavenumbers $k_2$ and $\kappa_{2j}$. For outwardly propagating second-order free waves

$$4\sigma^2 = gk_2 \tanh k_2 d \tag{13}$$

which was given in (9); while for the standing or evanescent wave modes, the wavenumbers are given by

$$4\sigma^2 = -g\kappa_{2j} \tan \kappa_{2j} d \tag{14}$$

which has infinitely many positive roots, $\kappa_{2j}$, given by

$$\left(j - \frac{1}{2}\right)\pi \leq \kappa_{2j} h \leq j\pi$$

The homogeneous solutions therefore consist of outwardly radiating second-order free waves as well as local standing waves, i.e. evanescent modes, both of which are determined to within a set of unknown constants. The unknown coefficients, $a_{n0}$ and $a_{nj}$, are then determined by satisfying the no-flow condition on the cylinder. This is accomplished with the same procedure that is used to obtain the first-order scattered wave solution, based on the orthogonality properties of $\cosh k_2(d+z)$ and $\cos \kappa_{2j}(d+z)$. The method is straightforward but lengthy; thus, it will not be given in detail in this paper.

The final solution at second-order is completely specified by combining the particular solutions in (8) and (10) with the complementary solutions obtained from (12) after evaluating the unknown coefficients. The solution for the second-order velocity potential is derived in detail by Kriebel (1987) and may ultimately expressed in closed integral form as

$$
\begin{aligned}
\Phi_2 = -\,i\frac{g(kH)^2}{2k\sigma} \sum_{n=0}^{\infty} \cos n\theta \\
\cdot \Bigg[ C_1 \cosh 2k(d+z)\beta_n J_n(2kr) - C_{10}C_0 \cosh k_2(d+z)\beta_n \frac{J_n'(2ka)}{H_n'(k_2a)} H_n(k_2r) \\
- \sum_{j=1} C_{1j}C_j \cos \kappa_{2j}(d+z)\beta_n \frac{J_n'(2ka)}{K_n'(\kappa_{2j}a)} K_n(\kappa_{2j}r) \Bigg] \\
+ \Bigg[ PV \int_0^{\infty} \frac{C_2}{k} \cosh \kappa(d+z) J_n(\kappa r) d\kappa - C_0 I_{20} \cosh k_2(d+z) \frac{H_n(k_2r)}{kH_n'(k_2a)} \\
- \sum_{j=1} C_j I_{2j} \cos \kappa_{2j}(d+z) \frac{K_n(\kappa_{2j}r)}{kK_n'(\kappa_{2j})} \\
+ C_3 C_0 \cosh k_2(d+z)\Big[ J_n(k_2r) - \frac{J_n'(k_2a)}{H_n'(k_2a)} H_n(k_2r) \Big] \Bigg] e^{-i2\sigma t}
\end{aligned}
\tag{15}
$$

where the nondimensional coefficients are defined as

$$
C_0 = \frac{\cosh k_2 d}{\sinh 2k_2 d + 2k_2 d} \qquad\qquad C_j = \frac{\cos \kappa_{2j} d}{\sin 2\kappa_{2j} d + 2\kappa_{2j} d}
$$

$$
C_1 = \frac{3}{4}\frac{k(\tanh^2 kd - 1)}{\cosh 2kd(2k\tanh 2kd - k_2\tanh k_2 d)}
$$

$$
C_{10} = 6\frac{k^2(\tanh^2 kd - 1)}{4k^2 - k_2^2} \qquad\qquad C_{1j} = 6\frac{k^2(\tanh^2 kd - 1)}{4k^2 + \kappa_j^2}
$$

$$
C_2 = \frac{1}{4}\frac{\kappa D_n(\kappa)}{\cosh \kappa d(\kappa \tanh \kappa d - k_2 \tanh k_2 d)}
$$

$$
I_{20} = \int_0^{\infty} \frac{\kappa^2 D_n(\kappa) J_n'(\kappa a)}{(\kappa^2 - k_2^2)} d\kappa \qquad\qquad I_{2j} = \int_0^{\infty} \frac{\kappa^2 D_n(\kappa) J_n'(\kappa a)}{(\kappa^2 + \kappa_{2j}^2)} d\kappa
$$

$$
C_3 = \frac{i\pi}{2}\frac{k_2}{k} D_n(k_2)
$$

In the solution given by (15), terms enclosed in the first bracket on the right hand side represent: (1) the forced Stokes plane wave component at wavenumber $2k$ and (2) the free cylindrical wave motion due to the scattering of this Stokes plane wave from the cylinder. These terms are found to be identical to a portion of the solution proposed by Chen and Hudspeth (1982), derived using the method of Green's functions. Terms in the second bracket then represent: (1) the remaining forced-radiated wave motion due to other nonlinear wave-wave interactions as well as (2) free scattered waves due to the interaction of these forced-radiated waves with the cylinder. Although derived in an independent way, the solution for these forced wave motions in (10) is identical to that proposed by Garrison (1979), also through application of Green's theorem, as Garrison's Green's function for the free surface potential can be reduced analytically to that given by (10) for a circular cylinder. Garrison then obtains the scattered wave solutions numerically in terms of a second Green's function and an unknown source distribution on the cylinder. The scattered wave motions in the proposed solution are obtained in closed-form based on the complete set of eigenfunction solutions for the homogeneous boundary value problem.

## SOLUTION FOR NONLINEAR FREE SURFACE

The first and second-order velocity potentials are substituted into the dynamic free surface boundary condition to evaluate the form of the free surface around the cylinder. Based on the perturbation expansion technique, $\Phi$ and $\eta$ are expanded in power series form, and the dynamic free surface boundary condition is then expanded in a Taylor series about the still water level, $z = 0$. The resulting expression for the water surface, consistent to the second perturbation order, may then be obtained as

$$\eta_1 + \eta_2 = -\frac{1}{g}\Phi_{1t} - \frac{1}{g}\Phi_{2t} - \frac{1}{g^2}\Phi_{1t}\Phi_{1tz} - \frac{1}{2g}\left[\Phi_{1r}^2 + \frac{1}{r^2}\Phi_{1\theta}^2 + \Phi_{1z}^2\right] \tag{16}$$

The resulting wave field, based on the right side of (16), is found to include: (1) linear incident and scattered waves, (2) second-order components from the second-order velocity potential, and (3) second-order components derived from nonlinear product terms of the first-order wave field. These last quadratic terms are found to include both steady components as well as components that oscillate at twice the frequency of the linear waves. All terms may be obtained from a straightforward substitution of the velocity potentials in (3) and (15) into (16); however, the results are quite lengthy and include several double-summations. The interested reader may refer to Kriebel (1987) for details.

In Figures 2 and 3, contours of wave crest amplitudes around the cylinder are shown for the linear and nonlinear diffraction solutions respectively. An example of the predicted wave crest and trough envelopes along the x-axis, as well as around the circumference of the cylinder, is then shown in Figure 4, where second-order mean water levels are also shown. In each figure, results are normalized by the incident wave amplitude and are given for a reference case where $ka = 1.0$, $kd = 1.57$, and where $kH = 0.5$. It is noted, however, that while the nonlinear solution in (15) and in Figure 3 is a function of $kH$, the nondimensional linear solution in (3) and in Figure 2 is not a function of the wave steepness.

In the up-wave region, the linear scattered wave opposes the linear incident wave to form a partial standing wave system. Second-order components generally increase the crest heights in the antinodes while reducing trough amplitudes. It is found, however, that terms from the second-order velocity potential in (10) are mostly out-of-phase with the linear solution and tend to decrease crest heights while other second-order components are in-phase and lead to the expected increase in crest heights. The nonlinear increase in crest heights is most pronounced on the up-wave cylinder boundary, where runup amplitudes are significantly increased relative to linear theory. Spatially varying mean water levels are also found which are the cylindrical analog to the "corrugated" mean water levels associated with standing waves in front of a vertical plane barrier. These components are superimposed upon the usual uniform set-down associated with the two-dimensional Stokes wave theory.

In the down-wave region, linear incident and scattered waves propagate in generally the same direction and do not generate strong quadratic interactions compared to the up-wave region. At second-order, however, scattered free waves and diffracted waves from the up-wave region propagate away from the cylinder in the down-wave region. These waves are superimposed on the linear waves and their bound second harmonics to produce spatially varying crest and trough envelopes, analogous to those produced by the superposition of first- and second-order free and forced waves in a wave flume. These interactions vary in both $r$ and $\theta$ such that significant diffraction patterns are obtained with localized areas of constructive and destructive wave interactions. One result of these interactions is that there is also significant recovery of the wave crest amplitude immediately behind the cylinder at second-order, something that is not predicted by the first-order diffraction theory.
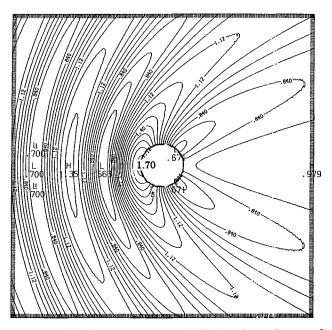
Figure 2. Wave crest amplitude contours for linear diffraction theory, for example case with $ka = 1.0$ and $kd = 1.57$.
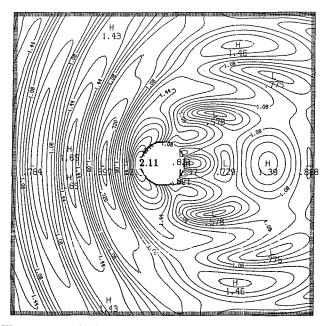


Figure 3. Wave crest amplitude contours for nonlinear diffraction theory, for example case with $ka = 1.0$, $kd = 1.57$, and $kH = 0.5$.
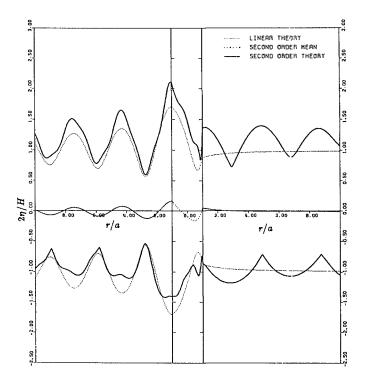
Figure 4. Wave crest and trough envelopes along x-axis, for example case with $ka = 1.0$, $kd = 1.57$, and $kH = 0.5$.

## EXPERIMENTAL VERIFICATION

The second-order diffraction theory is verified through comparison to laboratory data for: (1) wave runup and rundown envelopes around the circumference of the cylinder and (2) wave crest and trough envelopes along the x-axis out to a distance of 5 times the cylinder radius. The experiments were conducted in the directional wave basin at the University of Florida Coastal and Oceanographic Engineering Laboratory. The water depth was maintained at 45.0 centimeters with a cylinder radius of 16.25 centimeters, such that a constant depth-to-radius ratio of 2.77 was used for all experiments.

The experiments were conducted with monochromatic long-crested waves and a total of 22 experiments were carried out covering a broad range of the nondimensional parameters. Relative cylinder sizes remained in the diffraction regime with $ka$ values from 0.271 to 0.917. Relative water depths remained in the intermediate depth regime $kd$ values from 0.75 to 2.536. Values of the wave steepness were selected such that Stokes theory would remain convergent, although some waves with very high steepness were also tested; $kH$ values ranged from 0.085 to 0.806. Stokes second-order theory is formally expected to be appropriate for only 8 of the 22 experiments, while higher order wave theories would be most appropriate for the remaining conditions.

Wave runup data were obtained by video-taping the water surface on the circumference of the cylinder as waves passed a grid painted on the outside of the cylinder. Data analysis included selecting a 20 to 30 second period of steady state conditions and then averaging the wave crest runup and trough rundown for 10 waves every 15 degrees around the cylinder. For 12 of the experiments a video record was also made of waves passing a "photopole" array, which consisted simply of 10 thin vertical rods placed in a linear array along the $x$ axis as depicted in Figure 5. The photopole data consists of the wave crest and trough envelopes at each pole location, averaged over 10 waves. The photopole experiments were conducted separately from the runup experiments so that the presence of the poles would not disrupt the other measurements.
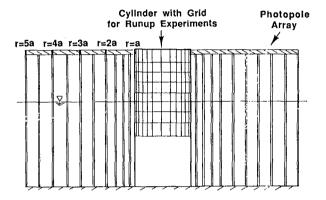
Figure 5. Experimental set up showing photopole array along x-axis.

Examples of the first- and second-order theories compared to laboratory wave runup and rundown data are shown in Figures 6 through 8. Based on a comparison of the data to linear theory, several general conclusions may be reached. Maximum wave runup at the front of the cylinder is greater than that predicted by linear theory in all cases and the runup distribution is poorly predicted by the linear theory. At the rear of the cylinder, the wave crest amplitude is also greater than that predicted by linear theory in all cases. Finally, the rundown amplitudes in the front and rear of the cylinder are not as large as predicted by linear theory.

In contrast, the nonlinear diffraction theory provides much better agreement for runup distributions and maxima. From Figure 6, for the smallest relative cylinder size and depth tested, the measured runup profile is almost exactly predicted over all angular positions by the second-order theory, even though this wave steepness is just at the limit of validity of Stokes theory where cnoidal theory may be more appropriate. The rundown envelope is well-predicted only over the rear half of the cylinder in this case.

For larger values of $ka$ and $kd$, second-order predictions for wave runup distributions are in good agreement with the data for conditions where Stokes second-order theory is expected to be valid. At higher values of $kH$, however, like that shown in Figure 7, the nonlinear theory predicts substantially larger runup than linear theory but still tends to underpredict the maximum runup. The rundown envelope is predicted fairly well at front and rear, however, the large trough amplitudes predicted near 75° are not displayed in the data, exect for waves of low steepness.

In Figure 8, the runup and rundown envelopes are predicted very accurately, this time even for a condition where Stokes 3rd or higher order theories are most appropriate and where the wave steepness is at nearly 70 percent of the theoretical breaking steepness. In this case, both the maximum runup at the front and at the rear are predicted almost exactly. The rundown distribution is also well-predicted over the leading half of the cylinder, but again is not well-predicted along the sides of the cylinder.
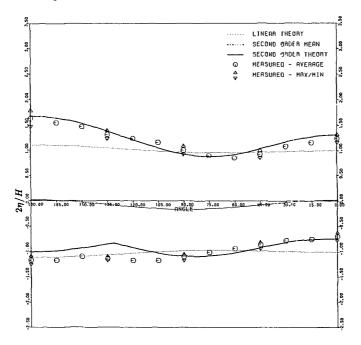


Figure 6. Example of wave runup distribution for $ka = 0.271$, $kd = 0.750$, and $kH = 0.215$.

In Table 1, the measured maximum crest runup is compared to both linear and nonlinear diffraction theories for all experiments. The results indicate that the maximum runup exceeds that predicted by linear theory by 13 to 83 percent and by 44 percent on average for the experimental data set. In contrast, the second-order theory overpredicts the maximum runup by 1 to 5 percent for the first set of conditions, predicts the measured runup to within 0 to 22 percent for most cases, and underpredicts by more than 40 percent for only two tests where the steepness was near breaking. In general, the data exceeds the nonlinear theory by 11 percent on average and by only 8 percent if the two conditions near breaking are excluded.
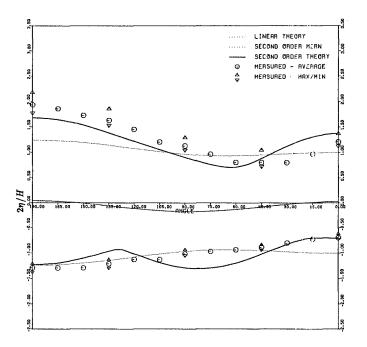
Figure 7. Example of wave runup distribution for $ka = 0.374$, $kd = 1.036$, and $kH = 0.286$.
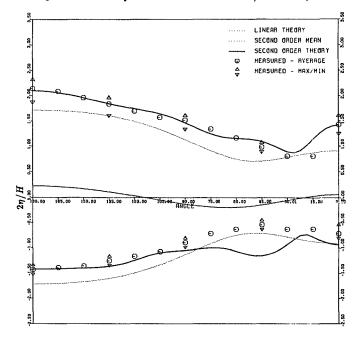


Figure 8. Example of wave runup distribution for $ka = 0.917$, $kd = 2.536$, and $kH = 0.631$.

Table 1. Experimental results for maximum wave runup

| $ka$ | $kd$ | $kH$ | % Diff. Linear | % Diff. Nonlinear |
|---|---|---|---|---|
| 0.271 | 0.750 | 0.132 | 27 | -2 |
|  |  | 0.178 | 36 | -5 |
|  |  | 0.215 | 48 | -1 |
| 0.308 | 0.853 | 0.085 | 16 | 1 |
|  |  | 0.137 | 33 | 5 |
|  |  | 0.182 | 45 | 6 |
|  |  | 0.250 | 65 | 13 |
|  |  | 0.296 | 78 | 13 |
| 0.374 | 1.036 | 0.122 | 13 | 0 |
|  |  | 0.205 | 36 | 15 |
|  |  | 0.286 | 56 | 19 |
|  |  | 0.385 | 69 | 16 |
|  |  | 0.402 | 76 | 18 |
| 0.481 | 1.332 | 0.186 | 13 | 7 |
|  |  | 0.317 | 20 | 4 |
|  |  | 0.438 | 35 | 9 |
|  |  | 0.530 | 80 | 40 |
| 0.631 | 1.745 | 0.683 | 61 | 22 |
| 0.684 | 1.894 | 0.391 | 18 | 5 |
|  |  | 0.572 | 43 | 22 |
| 0.917 | 2.536 | 0.631 | 25 | 0 |
|  |  | 0.806 | 83 | 43 |

Examples of the photopole experiments are presented in Figures 9 and 10. The visual observations of the wave crest and trough envelopes are compared to the first and second-order theoretical solutions, which have been extended out to $r = 10a$ to give a better indication of the overall scattering and diffraction patterns along the $x$ axis. In general, the photopole data seem to verify the general features of the wave envelopes predicted by the second-order theory. For the smaller cylinder size, in Figure 9, the second-order scattered waves lead to additional nodes and antinodes in the up-wave region compared to linear theory. The photopole data confirm the positions and magnitudes of these maxima and minima for both the wave crest and trough on the up-wave side. On the down-wave side, the second-order wave components do not produce significant modulations in the envelopes; and, to within measurement accuracy, the data verify this theoretical prediction as well.

The data in Figure 10, for the largest cylinder size tested, show that both the predicted and measured envelopes are similar to the linear envelope except that the crest elevations are increased while troughs are reduced. No secondary maxima are predicted in the envelopes, in contrast to the results at smaller values of $ka$. On the down-wave side, significant spatial modulation is predicted for this case. Data from the crest envelopes provide a rough verification of these nonlinear diffraction effects, as the presence and approximate spacing of the predicted envelope maxima and minima are confirmed, although the measured envelopes are more poorly defined.
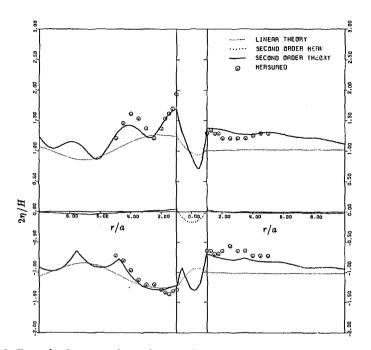
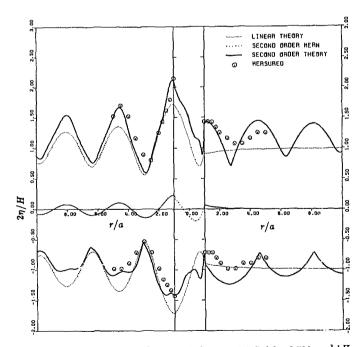Figure 9. Example of wave envelopes along x-axis for $ka = 0.374$, $kd = 1.036$, and $kH = 0.286$.

Figure 10. Example of wave envelopes along x-axis for $ka = 0.917$, $kd = 2.536$, and $kH = 0.631$.

CONCLUSIONS

The proposed second-order diffraction theory seems to rigorously account for nonlinear wave components including second-order forced waves due to nonlinearities in the free surface boundary condition as well as second-order free waves due to the nonlinear scattering process. Based on comparisons to laboratory data, the theory is then found to realistically predict the nonlinear characteristics of the wave field surrounding the cylinder. A comparison of the theory to previously proposed nonlinear diffraction theories shows substantial agreement in portions of the solution, but not in the entire solution, with the theories of Chen and Hudspeth (1982) and Garrison (1979). Finally, the proposed second-order theory seems to be valid for the same relative depth and wave steepness conditions for which the usual Stokes plane wave theory is valid.

REFERENCES

Chen, M.C., and Hudspeth, R.T., 1982, "Nonlinear Diffraction by Eigenfunction Expansion," *J. Waterway, Port, Coastal and Ocean Div.* , ASCE, Vol. 108, No. WW3.

Dean, R.G., and Dalrymple, R.A., 1984, *Water Wave Mechanics for Engineers and Scientists* , Prentice-Hall, Englewood Cliffs, New Jersey.

Garrison, C. J., 1979, "The Consistent Second-Order Theory of Wave/Structure Interaction," Naval Postgraduate School, Tech. Rpt. No. NPS-69-79-010, Monterey.

Hunt, J.N., and Williams, A.N., 1982, "Nonlinear Diffraction of Stokes Water Waves by a Circular Cylinder for Arbitrary Uniform Depth," *J. de Mechanique Theorique et Appliquee* , Vol. 1, No. 3.

Kriebel, D.L., 1987, "A Second-Order Diffraction Theory for Wave Runup and Wave Forces on a Vertical Circular Cylinder," Coastal and Ocean. Engr. Dept., Rpt. TR-072, University of Florida.

MacCamy, R.C., and Fuchs, R.A., 1954, "Wave Forces on Piles: A Diffraction Theory," U.S. Army Corps of Eng., *Beach Erosion Board* , Tech. Mem. No. 69.

Rahman, M., and Heaps, H.S., 1983, "Wave Forces on Offshore Structures: Nonlinear Wave Diffraction by Large Cylinders," *J. Phys. Ocean.* , Vol. 13.

Sabuncu, T., and Gören, O., 1985, "Second-Order Vertical and Horizontal Wave Forces on a Circular Dock," *Ocean Engr.* , Vol. 12, No. 4.

Wehausen, J. V., and Laitone, E.V., 1960, "Surface Waves," In *Encyclopedia of Physics* , ed. S. Flugge, Springer-Verlag, Berlin, Vol. IX.